Chinese Journal of Physiology 53(6): 439-446, 2010
DOI: 10.4077/CJP.2010.AMM029

Stochastic Model Shows How Cochlear Implants Process Azimuth in Real Auditory Space

Marek Drapal[1] and Petr Marsalek[1, 2, 3, 4]

[1]*Charles University of Prague, Department of Pathological Physiology*
U nemocnice 5, CZ-128 53, Praha 2, Czech Republic
[2]*Czech Technical University of Prague, Faculty of Biomedical Engineering*
Nam. Sitna 3105, CZ-272 01, Kladno, Czech Republic
[3]*Max Planck Institute for the Physics of Complex Systems*
Nöthnitzer Str. 38, D-011 87, Dresden, Germany
and
[4]*Czech Academy of Sciences, Institute of Physiology*
Videnska 1083, CZ-142 20, Praha 4, Czech Republic

Abstract

Interaural time difference (ITD) is a major cue for sound azimuth localization at lower sound frequencies. We review two theories of how the sound localization neural circuit works. One of them proposes labeling of sound direction in the array of delay lines by maximal response of the tuning curve (Jeffress model). The other proposes detection of the direction by calculating the maximum slope of tuning curves. We formulate a simple hypothesis from this that stochastic neural response infers sound direction from this maximum slope, which supports the second theory. We calculate the output spike time density used in the readout of sound direction analytically. We show that the numerical implementation of the model yields results similar to those observed in experiments in mammals. We then go one step further and show that our model also gives similar results when a detailed implementation of the cochlear implant processor and simulation of implant to auditory nerve transduction are used, instead of the simpli-fied model of auditory nerve input. Our results are useful in explaining some recent puzzling observations on the binaural cochlear implantees.

Key Words: coincidence detection, directional hearing, interaural time delay, stochastic neuronal model

Introduction

In previous studies we developed a stochastic model of the sound localization circuit (21-23). The work presented here aims to demonstrate that both simplified simulation of natural sound input and detailed simulation of cochlear implants (CI) yield a similar output in our binaural model. The goal of future work is an explanation of the tradeoff between complex sound recognition and localization observed in bilaterally implanted patients, as well as possible improvement of the CI stimulation protocols.

We present a model of sound localization in mammals. This model is consistent with new experimental findings of how the ITD (interaural time delay) is processed in mammals. In this paper we describe in more detail several key components of our model: neurons acting as coincidence detectors, spike timing jitter, random delays and other parameters, which can be identified with the biophysical properties of auditory neurons. We model the low frequency part of the sound localization circuit. Under the low

Corresponding author: Dr. Petr Marsalek, Charles University of Prague, Department of Pathological Physiology, U nemocnice 5, CZ-128 53, Praha 2, Czech Republic. Tel: +420-91080-6204, Fax: +420-22491-2834, E-mail: Petr.Marsalek@1f1.cuni.cz
Received: November 16, 2009; Revised: February 26, 2010; Accepted: March 3, 2010.
 ISSN : 0304-4920. http://www.cps.org.tw

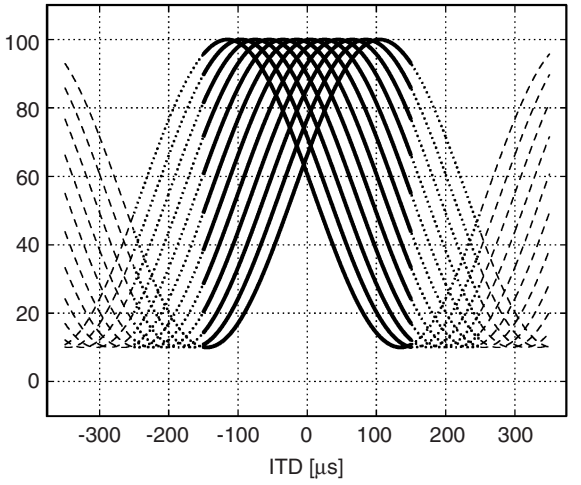

Fig. 1. Schematic responses of binaural neurons in the delay line (laminar nucleus). This and the following Figure show activities in the percentage of maximal activity (on the y-axis) of two respective types of binaural neurons of two respective neural circuits (avian in this Figure and mammalian in the next) in response to different values of the ITD in microseconds (on the x-axis). There are three bands for the ITD tuning corresponding to different line weights. The thick solid lines show the interval of the ITDs corresponding to the azimuth and based on the head size. The dotted lines show the interval outside the ITDs, which can be also used for the azimuth calculation. The dashed lines correspond to the continuation of the ITD for the next phase differences due to the continuity of the phase information. This Figure shows a set of twelve representative curves corresponding to the set of twelve neurons of the delay line (13) tuned by their maximal response to particular ITDs, 20 μs apart. This tuning corresponds to the position of the neuron within the delay line.

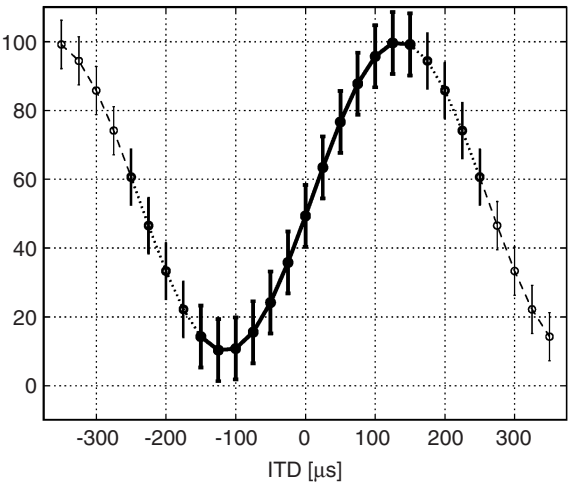

Fig. 2. Schematic responses of binaural neurons in the mammalian circuit (MSO). For axes and details see the caption for the previous Figure. The information about the azimuth is extracted from at least two (or possibly more) tuning curves of broadly tuned delay channels (10). Only one of the two channels is shown here. Error bars illustrate the stochastic dimension of the tuning: the actual response varies from trial to trial and the exact azimuth is extracted by pooling the signal from a small set of neurons.

frequency part we understand that part of the animal's hearing range, in which the ITD cue is used. The disparity of the inputs between the two ears is called interaural and the neurons, which have access to the spikes originating from both ears are called binaural. Our model describes the first binaural neurons found when progressing from periphery. There are analogous binaural neurons in birds (neurons of nucleus laminaris) and in mammals (neurons of superior olive), yet they are embedded in different neural circuits (7, 15). The level of description used in our paper is therefore the level of the neural circuit for the ITD processing.

Both the avian and mammalian circuits are subject to continuous experimentation (10). The experiments are demanding because stimuli have to have high time precision in the microsecond range and because the neural circuits are in intimate proximity of centers of animal's vital functions. Experimental literature is now available with detailed discussion of both these circuits (3, 7). We can take the experimental description of these neural circuits and use them as a testing ground for the theories conveying how sound is encoded into spike trains in lower processing stages of the auditory pathway.

Theories of how these circuits might function have long been presented and compared to experimental data. The first theory suggested that the ITD's are processed by a delay line. This was proposed by Jeffress in 1948 (13). Only several decades later it was demonstrated by experiments on barn owls that a variant of delay line exists in a neural circuit of the barn owl and also that line was found in other birds (7, 10). The neural circuit of birds converges on the binaural nucleus laminaris.

Even though several experimentalists have attempted to find a structure similar to avian delay line in mammals, the results are not conclusive (15). We described necessary and suffcient properties of binaural neurons to make them able to use the information contained in the ITD (21). New experimental findings indicate that a mammalian sound localization circuit may be wired differently than the avian (10). McAlpine and colleagues (24) also presented several purely theoretical works, amongst them reference No. 11, in which they explain some properties of the ITD coding by a neural population. Some of the coding properties are shared by both avian (Fig. 1) and mammalian (Fig. 2) circuits. We described neural

operations of the coincidence detection circuits in terms of random spike arrivals and their probability densities (23). We followed up with more estimates, in particular studying the standard deviation of spike timing, sometimes called spike timing jitter (17, 22).

Model

The integrate and fire neuronal model, also called the perfect integrator, is one of the simplest neural models. This model captures the integration property of a neuron, especially for time scales shorter than the neuronal time constant. The time constant can be measured electro-physiologically and especially in auditory neurons it can be assumed to be large compared to the rate of synaptic inputs. With a given integration time window and complex input, such a neuronal model possesses rich output behavior, which can be attributed to hypothetical neural computations (9, 31). In agreement with our notation in reference No. 17 the neural computations of the perfect integrator can be summarized as:

$$\left.\begin{array}{c} 1\text{-st input} : f_{\text{in}}(t) \\ \vdots \\ n\text{-th input} : f_{\text{in}}(t) \end{array}\right\} \rightarrow \text{first } (k) \text{ spikes} \rightarrow f_{\text{out}}(t), \quad [1]$$

where f_{in} are input spike timing densities, f_{out} is the output density, k is the number of spikes needed to fire the action potential and n is the total number of inputs. Here we consider only small amounts of input spikes, k, n = 2, 3, 4 and a short time integration window Δ_{W}. Due to the short time window, such a neuron acts as a coincidence detector. We will see that the neural computation performed by this model is quite complex.

The mammalian brainstem neural circuitry is shown in Fig. 3. Since there is chain of delays on both sides at each synapse, we can generally suppose that we have n ipsilateral delays in the ipsilateral (A) branch of the pathway, $\Delta_{\text{A}1}$, $\Delta_{\text{A}2}$, ..., $\Delta_{\text{A}n}$ and m contralateral delays in the contralateral (B) branch of the pathway, $\Delta_{\text{B}1}$, $\Delta_{\text{B}2}$, ..., $\Delta_{\text{B}m}$. The total delay difference between those two pathways, Δ_{AB}, is equal to

$$\Delta_{\text{AB}} = \Delta_{\text{AJ}} - \Delta_{\text{BJ}} = \sum_{i=1}^{n} \Delta_{\text{A}i} - \sum_{j=1}^{m} \Delta_{\text{B}j}. \quad [2]$$

We assume that these random delays with (timing) jitter (subscript J) on sides A and B (left and right) are mutually independent and identically distributed non-negative random variables. We denote them as Δ_{AJ}, Δ_{BJ} with a maximum value of Δ_{max}. The following constraints have to be imposed on them, with the third reflecting the property that the coincidence detection (time) window Δ_{W} should be shorter

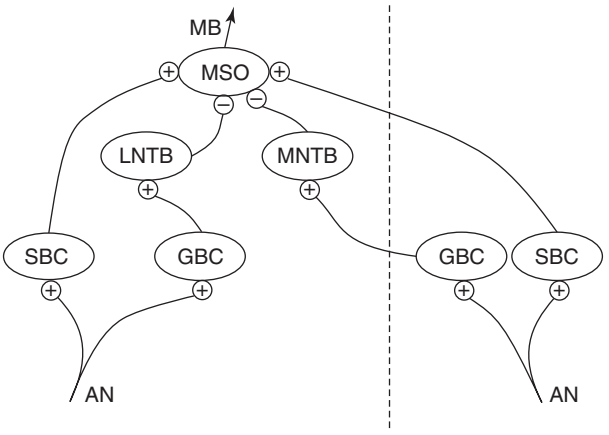

Fig. 3. Mammalian brainstem wiring. This scheme shows synaptic connections in the mammalian brainstem converging onto the nucleus of the medial superior olive (MSO) and passing the spike trains further to the midbrain (MB). Vertical line denotes the dividing mid line between the left and right brainstem sides. Only one half of the circuit converging to the left MSO is shown. The neurons of the processing stages from bottom to top are: neurons of the ganglion spirale, also known as auditory nerve (AN) neurons, neurons of the cochlear nuclei, namely globular bushy cells (GBC) and spherical bushy cells (SBC). Input of the former is inverted through the medial (MNTB) and lateral nuclei of trapezoid body, while input of the latter connects directly to the MSO. The polarity of synapses is denoted by the plus (+) sign for excitatory and minus (-) sign for inhibitory.

than or equal to the maximum delay, and that the sound period T should be greater than or equal to the maximum delay:

$$0 \le \Delta_{\text{JA}} \le \Delta_{\text{max}}, \quad 0 \le \Delta_{\text{JB}} \le \Delta_{\text{max}},$$
$$0 \le \Delta_{\text{W}} \le \Delta_{\text{max}} \le T. \quad [3]$$

These are the theoretical conditions which have to be met to solve the analytical calculation. Using numerical simulations we verify that the model is robust in parameter variations within these conditions. Some of the extrapolated values mimic the phase ambiguity observed in the auditory experiments.

Let us substitute to Equation [1] n = 2 and for the spike timing probability density f_{in} the beta distribution. Such a spike timing is observed in the auditory pathway (18). The beta distribution has a probability density function written as:

$$f_{\text{in}}(t) = \frac{1}{B(a, b)} H(t) H(1-t) t^{a-1} (1-t)^{b-1}, \quad [4]$$

with parameters a, $b \ge 1$, normalized by $B(a, b)$ to give unity integral. $B(x, y)$ and $\Gamma(x)$ are respectively (Euler) beta and gamma functions and can be cal-

culated as $B(x, y) = \Gamma(x)\Gamma(y)/\Gamma(x + y)$ and $\Gamma(x) = \int_0^\infty t^{x-1}\exp(-t)dt$ (1). $H(x)$ is the (Heaviside) step function: $H(x) = \begin{cases} 0, & \text{for } x < 0, \\ 1, & \text{for } x \geq 0. \end{cases}$ The mean, standard deviation and variation coeffcient, of the beta distribution expressed in parameters a and b are:

$$\mu = \frac{a}{a+b}, \quad \sigma = \sqrt{\frac{ab}{(a+b)^2(a+b+1)}},$$

$$C_V = \sqrt{\frac{b}{a(a+b+1)}}, \qquad [5]$$

respectively. For $a = b = 1$ the beta distribution in Equation [4] is the uniform distribution and for $a = 1$ and $b = 2$ it is the triangular distribution.

Results

Analytical Calculations

For two independent random variables Δ_{AJ} and Δ_{BJ} we can obtain a new random variable defined as a difference in Equation [2]. The convolution formula for the sum of the two random variables Δ_{AJ} and $-\Delta_{BJ}$ with distributions f_{inA} and f_{inB} prescribes that distribution f_{out} of this new variable Δ_{AB} is written as convolution integral

$$f_{out} = f_{inA} * f_{inB}. \qquad [6]$$

For the evaluation of this convolution formula we can use the property of the Laplace integral transform (30) that it replaces the convolution operation ($*$) with multiplication ($\cdot$).

$$L\{f_{inA} * f_{inB}\} = L\{f_{inA}\} \cdot L\{f_{inB}\}. \qquad [7]$$

We obtain the sought distribution f_{out} by means of the inverse Laplace transform:

$$f_{out} = L^{-1}\{L\{f_{inA}\} \cdot L\{f_{inB}\}\}. \qquad [8]$$

Let us substitute f_{inA} and f_{inB} in this Equation with the beta distribution [4], $f_{inA} = f_{in}(t)$ and $f_{inB} = -f_{in}(1 - t)$. We can use the properties of the Laplace transform that it is a linear operator and can have as an argument the unit step (Heaviside) function. Even though the two unit steps define the function in three pieces, the symbolic manipulation software we used, the MATLAB(TM) symbolic toolbox, calculates the output function seamlessly. One of the simplest nontrivial examples is to set $a = 2$ and $b = 4$ in formula [4]. In this example, f_{in} is the 4th degree polynomial, $\sum_0^4 c_i t^i$, such that the output of the convolution will be the 9th degree polynomial:

$$f_{out}(t) = \begin{cases} -c_9t^9 - c_8t^8 + c_7t^7 - c_6t^6 + c_5t^5 - c_4t^4 + c_3t^3 - c_2t^2 + c_1t^1 + c_0, & 0 \leq t \leq 1, \\ +c_9t^9 - c_8t^8 - c_7t^7 - c_6t^6 - c_5t^5 - c_4t^4 - c_3t^3 - c_2t^2 - c_1t^1 + c_0, & -1 \leq t \leq 0, \\ 0, & \text{otherwise}, \end{cases} \qquad [9]$$

where the absolute values of the polynomial coeffcients are $c_9 = 0.6349$, $c_7 = 2.8571$, $c_4 = 20$, $c_3 = 33.33$, $c_2 = 17.1429$, $c_0 = 1.5873$, $c_8 = c_6 = c_5 = c_1 = 0$ and signs are as denoted. The signs of the coeffcients confirm that this polynomial is an even function.

In this way we arrived at the formula for the excitatory coincidence detection (23). When we add inhibition, from Equation [9] we obtain the inhibitory coincidence detection function as a new density f_{out} obtained by the difference of the excitatory f_{exc} and the inhibitory f_{inh} inputs,

$$f_{out}(t) = f_{exc}(t) - f_{inh}(t - T_\phi) + C. \qquad [10]$$

T_ϕ corresponds to a phase shift, and C is a baseline firing rate to get nonnegative firing. The two ITD tuning curves with and without inhibition in Fig. 7 can be compared to experiment in Ref. No. 3. To highlight the differences between the distributions discussed here, Fig. 5 shows f_{in} of Equation [4] and f_{out} of Equation [9], compared to normal density $N(0, \sigma)$ with the standard deviation σ set equal to the standard deviation of f_{out}. In order to see the differences in their tails, these functions are shown in both semi-logarithmic and linear scales.

Numerical Calculations

In this section we briefly present implementation details of the model in Fig. 4. The latencies are simulated together with the stochastic arrival of spike at the first binaural neuron. We used several modifications of the model. We are now in a process of rigorously showing that some of the model variants are computationally equivalent. We use both inhibitory and excitatory inputs to the binaural neuron. This is

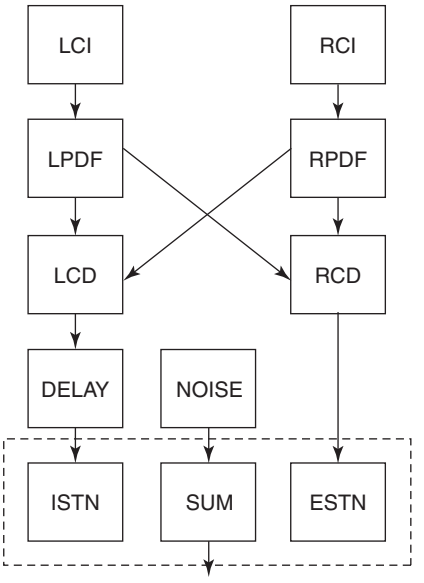

Fig. 4. Model circuitry. L and R CI are left and right cochlear natural or cochlear implant inputs. L and R PDF are analogously left and right probability density functions of spike generation times. L and R CD are coincidence detector neurons. This is an analogue to the processing at the first binaural neuron. DELAY is the axonal conduction delay and is shown only for the inhibitory branch. I and ESTN are inhibitory and excitatory synaptic transmissions, which are summed as the SUM of synaptic inputs together with NOISE. It can be shown that this circuitry is equivalent to the simplified wiring of the mammalian sound localization circuit, as described for example in reference No. 10.

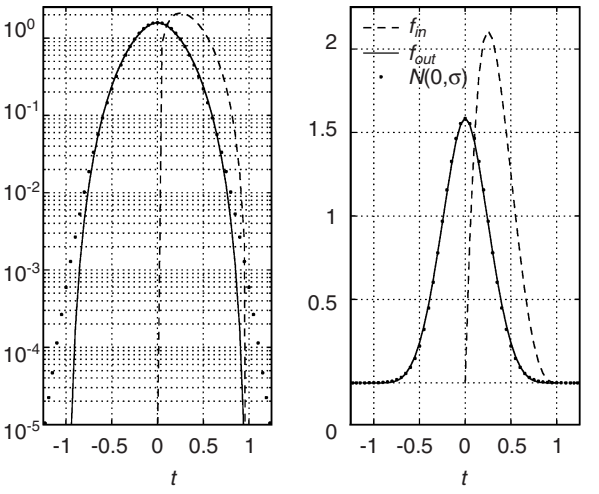

Fig. 5. Input and output probability density functions. The semi-logarithmic plot used in the left panel shows the divergence of the two tails of the normal and beta densities, as the tail of the normal density ($N(0, \sigma)$, dots) exceeds the range below the argument of -1 and above that of 1. Semi-logarithmic plotting on the y-axis of the densities was used in the past, because the normal density is parabolic in these coordinates. In the right panel, the densities are shown on a linear scale for a more conventional comparison. Note that dots of the normal density virtually fall on the solid curve of the beta density in the linear panel. Standard deviation of the normal density σ was chosen to be equal to standard deviation of the output density f_{out}. The dashed line shows the input density f_{in} and the solid line shows the output density f_{out} on the whole interval, see Equation [9].

consistent with the mammalian literature (10, 11, 24). Our model makes it possible to describe neural coding in lower stages of auditory processing and therefore the model can be used for studying both natural and electronic sensation, the latter evoked by cochlear implant stimulation (20).

We can recalculate the input to the auditory nerve by a cochlear implant emulator. We use a published and publicly available realistic software emulation of cochlear implant adapted from an open source in the MATLAB(TM) script language by Bruce and several other authors (4-6, 34). We then convert the CI signal into auditory nerve activity using a method implemented by these authors (6).

In the last decade, many deaf patients in Europe have received implants in both cochleas from the same manufacturer. Existing technology enables synchronized stimulation of both cochleas in these patients. Cochlear implants can switch between several coding strategies, some useful for speech understanding and some other useful for open space hearing. In the Nucleus (R) 24 cochlear implant system common coding strategies are Spectral Peak (SPEAK), Continuous Interleaved Sampling (CIS) and Advanced Combination Encoder (ACE) (8). In our example we choose the SPEAK strategy (8, 25). Figure 6 shows successive steps of sound processing in the emulator. Only the channel with the highest energy out of more than twenty frequency channels of the CI model is shown.

It has been shown previously in experiments that there exists a trade-off between sound localization and speech comprehension in these patients (8). Another finding demonstrates that specific types of spike timing jitter are beneficial in these patients (19). In our work we demonstrate theoretically, why different types of jitter are useful. The improvements of our sound localization model may lead to the formulation of novel neural coding strategies for cochlear implants. Figure 7 shows data obtained in the CI emulator together with our model. On the x-axis is the interaural time delay between left and right inputs.

Discussion

Our results do not exclude the possibility that

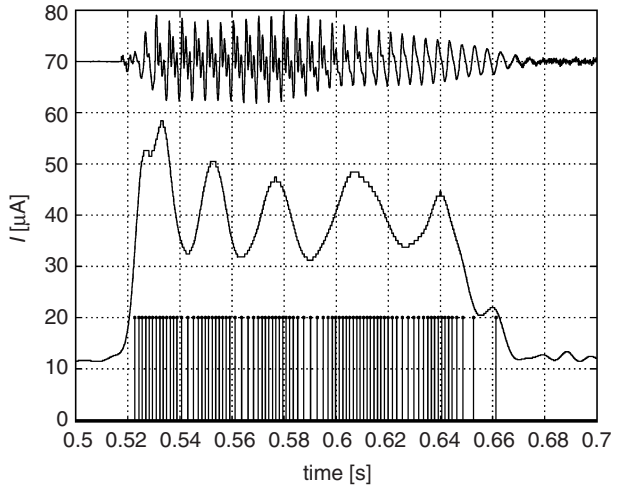

Fig. 6. Output example. Spikes in the auditory nerve are elicited by the current from the cochlear implant. The x-axis shows a time span of 200 ms. The upper trace shows complex speech sound in auditory space. This is a Czech syllable pronounced by a Czech native speaker. The units on the y-axis (μA) are related to the middle trace, which shows the stimulation current evoked by the sound. The bottom trace is a spike train elicited in a channel of cochlear implant with the highest energy content.

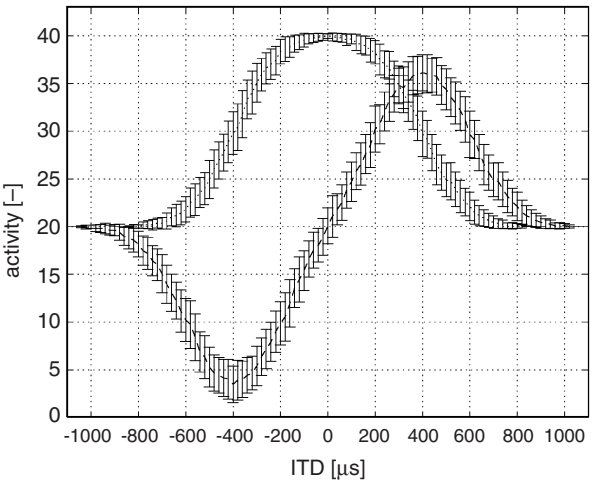

Fig. 7. Output of binaural model neuron. The model neuron is connected to the whole CI simulation package. ITD is on the x-axis in microseconds. Neuronal output activity is plotted on the y-axis. The dashed biphasic curve is the output of the full model with both excitation and inhibition. The dotted monophasic curve is the model without inhibition. Only one period of the output is shown on this picture for clarity, but the output is periodic, hence the x-axes could be easily converted to the interaural phase difference. The error bars are sample standard deviations obtained numerically in simulations. In both curves they are the result of 100 trials. In other words, these error bars do not show the level of the noise in the system. Instead, the noise is introduced into the system *via* the randomness of the random variables and the magnitude of the timing jitter.

arrays of delay lines in the auditory brainstem neural circuit exist in mammals. We are only offering an alternative solution to the well known problem of time precision in sound localization. Our alternative solution is based on the concept of only one delay line. It is possible that the real neural circuit lies between these two extreme alternatives. More specifically, the circuit of the MSO might use a few channels tuned to specific ITDs. The continuum of the ITDs would be then represented in analogy to the continuum of colors, which is represented in the activity of three channels corresponding to just three cone pigments. ITD can be detected for both low frequency sounds and also for the envelopes of the amplitude modulated sounds (14).

All neural circuits extracting precise timing information must employ coincidence detectors. Output of these coincidence detectors can be passed with even higher timing precision to the next order neurons in auditory pathway (28). Precise spike timing is preserved even in higher relays of the auditory pathway, up to the thalamus and cortex, (27, 32), yet the function of such precisely timed spikes in the cortex is not known.

An important point for the interpretation of experimental data is the following. When looking at the experimental data, one cannot distinguish which of the two similar densities (with and without the tails, see Fig. 5) govern the data. We exemplified this in (22), where we demonstrated that the sample data of output density without the tails pass the Jarque-Bera (2) normality test with the confidence level p lower than any practically used value. Since publishing this finding (22), we have a more precise explanation as to the implications of the result of the Jarque-Bera test. Mathematically, the two densities differ because of their tails. Practically, when analyzing data or numerically simulated data samples, one data density cannot be distinguished from the other. It is important to realize that the output density is the density of timing jitter of the MSO neuron, and that the spike encoding this randomness is entering another neuron. The interpretation of data of spike timing density using the normal density is a common practice and it is not necessarily wrong. The difference we report here is subtle, but may matter for the proper description of the neural algorithm.

While the size of the CD window can be regulated in the neural circuit, the time jitter can also change based on the other parameters of the circuit, (28). Our results show that the proposed mechanism is robust to variation of these two parameters (time window and

time jitter).

Figures 1 and 2 hint at how various ranges of ITDs might be processed in mammals with various head sizes. To demonstrate this theoretical result in experiment might be diffcult, but it is not impossible. Implanting two cochlear implants in both cochleas of a monkey and also in a guinea pig for comparison based on varied timing jitter is one suggestion for a demanding, yet realizable experiment.

It is also interesting to know that another type of the ITD jitter was already used in a variant of a human psychophysical experiment. A controlled neural jitter influences the sound localization performance, as reported in reference No. 19. This experiment is measurement of the sound localization performance of hearing impaired human volunteers. These implantees, who have cochlear implants on both sides, are capable of the ITD processing. In short, it is interesting to consider the working hypothesis of this paper, stating that the jittered binaural stimulation abolishes the adaptation at the binaural processing stage as opposed to the stimulation without time jitter. We can compare this hypothesis to what we know about the circuit. We would like to comment that the observation in reference No. 19 might also be explained by the active use of timing jitter by neurons, as proposed here. In the psychoacoustics of normal hearing subjects, this might be indirectly illustrated by careful manipulation of echoes and distractors, (16), but the interpretation of these experiments from the point of view of our theory is less straightforward.

Our model circuit does not reflect the detailed anatomical wiring of the real circuit because the real wiring is far too complex. In designing our model we started with the detailed circuit description. Any physiological description uses elementary neural operations: delay, summing of the postsynaptic potentials, coincidence detection, which can be understood as an operation of the "and" binary logical gate and inhibition, which can be understood as the "not" unary operation. Starting from the (complex) neural circuit, we can simplify it, when simplification of the series of operations is possible. Our model is the result of such a simplification. We can prove that the original and simplified circuits are equivalent from the computational perspective (22). It should be also noted that whenever (slow) software implementation would not make the real-time implementation possible immediately, most computations can be implemented using (much faster) digital signal processing hardware. We refer here to the hardware model of the interaural level difference processing in bats (12) as one out of many examples.

The neural circuits which use coincidences of two inputs and calculate the correlation between the two neural signals have a long tradition following the Reichardt detector, a neural circuit for motion detection in fly vision (29, 33). In line with this tradition, early applications of neural correlations in sound localization circuits involved the possibility that not the peak, but the maximal slope of a response of the coincidence detector may relay the information, (26).

Figure 4 shows the neural operations as individual functional building blocks of a neural algorithm, which should not be mapped directly to neurons of the binaural pathway in Fig. 3. The spike timing jitter propagates through all the neurons of the ascending auditory pathway. In this paper we demonstrated, why a specific type of spike timing jitter is essential for azimuth processing in both normal hearing and hearing with cochlear implants.

Acknowledgments

This work was supported by the research projects MSM 0021620806 and MSM 6840770012 granted by the Ministry of Education, Youth and Sports of the Czech Republic. Thanks to Zbynek Bures, Abigail Klopper, Paul Poon and Martin Vondrasek.

References

1. Abramowitz, M. and Stegun, I. Handbook of Mathematical Functions, With Formulas, Graphs, and Mathematical Tables, New York: Dover, 1965.
2. Bera, A. and Jarque, C. Effcient tests for normality, heteroscedasticity and serial independence of regression residuals: Monte Carlo evidence. *Econ. Lett*. 7: 313-318, 1981.
3. Brand, A., Behrend, O., Marquardt, T., McAlpine, D. and Grothe, B. Precise inhibition is essential for microsecond interaural time difference coding. *Nature* 417: 543-547, 2002.
4. Bruce, I.C., Irlicht, L.S., White, M.W., O'Leary, S.J., Dynes, S., Javel, E. and Clark, G.M. A stochastic model of the electrically stimulated auditory nerve: Pulse-train response. *IEEE Trans Biomed. Eng.* 46: 630-637, 1999.
5. Bruce, I.C., White, M.W., Irlicht, L.S., O'Leary, S.J. and Clark, G.M. The effects of stochastic neural activity in a model predicting intensity perception with cochlear implants: Low-rate stimulation. *IEEE Trans Biomed. Eng.* 46: 1393-1404, 1999.
6. Bruce, I.C., White, M.W., Irlicht, L.S., O'Leary, S.J., Dynes, S., Javel, E. and Clark, G.M. A stochastic model of the electrically stimulated auditory nerve: Single-pulse response. *IEEE Trans Biomed. Eng.* 46: 617-629, 1999.
7. Carr, C.E. and Konishi, M. Axonal delay lines for time measurement in the owl's brainstem. *Proc. Natl. Acad. Sci. U.S.A.* 85: 8311-8315, 1988.
8. Clark, G.M. Personal reflections on the multichannel cochlear implant and a view of the future. *J. Rehabil. Res. Devel*. 45: 651-694, 2008.
9. Gerstner, W., Kempter, R., van Hemmen, J.L. and Wagner, H. A neuronal learning rule for sub-millisecond temporal coding. *Nature* 383: 76-78, 1996.
10. Grothe, B. New roles for synaptic inhibition in sound localization. *Nat. Rev. Neurosci*. 4: 540-550, 2003.
11. Harper, N.S. and McAlpine, D. Optimal neural population coding of an auditory spatial cue. *Nature* 430: 682-686, 2004.
12. Horiuchi, T. and Hynna, K. Spike-based VLSI modeling of the

ILD system in the echolocating bat. *Neural Networks* 14: 755-762, 2001.
13. Jeffress, L.A. A place theory of sound localization. *J. Comp. Physiol. Psychol.* 41: 35-39, 1948.
14. Joris, P.X., Schreiner, C.E. and Rees, A. Neural processing of amplitudemodulated sounds. *Physiol. Rev.* 84: 541-577, 2004.
15. Joris, P.X., Smith, P.H. and Yin, T.C.T. Coincidence detection in the Auditory system: 50 years after Jeffress. *Neuron* 21: 1235-1238, 1998.
16. Kopco, N., Best, V. and Shinn-Cunningham, B.G. Sound localization with a preceding distractor. *J. Acoust. Soc. Am.* 121: 137-152, 2007.
17. Kostal, L. and Marsalek, P. Neuronal jitter: Can we measure the spike timing dispersion differently? *Chinese J. Physiol.* 53(6): 454-464, 2010.
18. Krishna, B.S. A unified mechanism for spontaneous-rate and first-spike timing in the auditory nerve. *J. Comput. Neurosci.* 13: 71-91, 2002.
19. Laback, B. and Majdak, P. Binaural jitter improves interaural time-difference sensitivity of cochlear implantees at high pulse rates. *Proc. Natl. Acad. Sci. U.S.A.* 105: 814-817, 2008.
20. Loizou, P.C. Introduction to cochlear implants. *IEEE Eng. Med. Biol. Mag.* 18: 32-42, 1999.
21. Marsalek, P. Coincidence detection in the Hodgkin-Huxley equations. *Biosystems* 58: 83-91, 2000.
22. Marsalek, P. and Drapal, M. Mechanisms of Coincidence Detection in the Auditory Brainstem: Examples, in: Mathematical Modeling of Biological Systems, edited by A. Deutsch, R. Bravo de la Parra, R. de Boer, O. Diekmann, P. Jagers, E. Kisdi, M. Kretzschmar, P. Lansky and H. Metz, volume 2, 255-264, Birkhaeuser, 2008.
23. Marsalek, P. and Lansky, P. Proposed mechanisms for coincidence detection in the auditory brainstem. *Biol. Cybern.* 92: 445-451, 2005.
24. McAlpine, D., Jiang, D. and Palmer, A.R. A neural code for low frequency sound localization in mammals. *Nat. Neurosci*. 4: 396-401, 2001.
25. Millar, I.B., Tong, Y.C. and Clark, G.M. Speech processing for cochlear implant prostheses. *J. Speech Lang Hear Res*. 27: 280-296, 1984.
26. Phillips, D.P. and Brugge, J.F. Progress in neurophysiology of sound localization. *Annu. Rev. Psychol.* 36: 245-274, 1985.
27. Poon, P.W.F. and Chiu, T.W. Similarities of FM and AM receptive space of single units at the auditory midbrain. *Biosystems* 58: 229-237, 2000.
28. Reed, M.C., Blum, J.J. and Mitchell, C.C. Precision of neural timing: Effects of convergence and time-windowing. *J. Comput. Neurosci.* 14: 35-47, 2002.
29. Reichardt, W. Nervous integration in the facet eye. *Biophys. J.* 2: 121-143, 1962.
30. Rektorys, K. (editor) Survey of Applicable Mathematics, London: Iliffe Books, 1969.
31. Vaillant, J. and Lansky, P. Multidimensional counting processes and evoked neuronal activity. *IMA. J. Math. Control Inf.* 17: 53-73, 2000.
32. Villa, A.E. and Abeles, M. Evidence for spatiotemporal firing patterns within the auditory thalamus of the cat. *Brain Res*. 509: 325-327, 1990.
33. Zanker, J.M., Srinivasan, M.V. and Egelhaaf, M. Speed tuning in elementary motion detectors of the correlation type. *Biol. Cybern.* 80: 109-116, 1999.
34. Zhou, Y., Carney, L.H. and Colburn, H.S. A model for interaural time difference sensitivity in the medial superior olive: Interaction of excitatory and inhibitory synaptic inputs, channel dynamics, and cellular morphology. *J. Neurosci.* 25: 3046-3058, 2005.